How a Conductive Baffle Improves Melting Characteristic and Heat Transfer in a Rectangular Cavity Filled with Gallium

Rouhollah Yadollahi Farsani[1,*], Amirhoushang Mahmoudi[2], Mehdi Jahangiri[1]

[1]Department of mechanical engineering, Shahrekord Branch, Islamic Azad University, Shahrekord, Iran.

[2]Department of Thermal and Fluid engineering, University of Twente, Enschede, The Netherlands.

[*]Corresponding Author, Email: R.Yadollahi@iaushk.ac.ir

Abstract: The configuration of a latent heat thermal energy storage (LHTES) is an important factor considered by manufacturers of heat storage systems. In this study, an applicable and low-cost way of improving melting behavior in a rectangular cavity was remarked. There was a preconceived idea that with a single conductive baffle, embedded on the upper wall of the cavity, the melting rate and the amount of heat storage could improve. Therefore, for different locations as well as lengths of a baffle, the heat transfer and melting characteristic of gallium as a phase change material (PCM) in a rectangular cavity were investigated numerically. The cavity has the insulated upper and bottom walls. The sidewalls are regarded to have constant temperatures one higher and another lower than the melting point of gallium. The phase change process is modeled with the fixed grid-based enthalpy-porosity method coupled with the semi-implicit method for pressure-linked equations (SIMPLE) algorithm. The isotherm lines and streamlines, as well as the liquid fraction and Nusselt number on the hot wall, are considered to present the results at a constant Rayleigh number equal to 10^6. The results show the baffle imposes noticeable improvement on the melting process of gallium in a rectangular cavity by influencing the feature of convective heat transfer. Investigating the different baffle's locations (LX/L=0.2 to 0.9) revealed that when the baffle located at the right half of the cavity, melting initiates from the left side, the more amount of PCM melts in comparison with the other cases. Ultimately, the dimensionless location of LX/L=0.8 demonstrates the best melting characteristic and the most final liquid fraction. The more liquid-fraction, the more energy storing concluded. It also observed a dimensionless height of LY/L=0.4 represents the most liquid-fraction compared to the heights of LY/L=0.2,0.3, and 0.4.

Keywords: Melting, Heat storage cavity, Conductive baffle, Convective Heat Transfer, PCM.

Nomenclature

b	enthalpy-porosity coefficient, $kgm^{-3}s^{-1}$	T_h , T_c	hot and cold temperatures, ^oC
B	dimensionless enthalpy-porosity coefficient	t	time, s
c	specific heat, $Jkg^{-1o}C^{-1}$	tx	baffle thickness
f	liquid fraction	u,v	velocity in the x,y direction, ms^{-1}
Fo	Fourier number	U,V	dimensionless velocity
g	gravity, $9.81ms^{-2}$	x,y	Cartesian coordinate, m
h	enthalpy, $Jkg^{-1}\,^oC^{-1}$	X,Y	dimensionless Cartesian coordinate
h_l	melting latent enthalpy, $Jkg^{-}\,^oC^{-1}$	***Greek Symbols***	
L,H	cavity dimension in x,y direction, m	α	thermal diffusivity, $k_f/\rho c_f$, m^2s^{-1}
LX,LY	baffle location and length	β	expansion coefficient, $^oC^{-1}$
k	thermal conductivity, $Wm^{-1}\,^oC^{-1}$	μ	dynamic viscosity , $N\,sm^{-2}$
Nu_{avg}	average Nusselt number	ν	kinematic viscosity, m^2s^{-1}
Nu_Y	local Nusselt number	θ	dimensionless temperature
p	pressure, $N\,m^{-2}$	ρ	density, kgm^{-3}
P	dimensionless pressure	σ	electrical conduction, Sm^{-1}
Pr	Prandtl number	***Subscripts***	
R	aspect ratio (Height/Length)	f,s	fluid and solid
Ra	Rayleigh number	l	melting point
Ste	Stefan number	CLF	cavity liquid fraction
T	temperature, ^oC	LHTES	latent heat thermal energy storage
T_l , T_s	melting and solidification points, ^oC		

1. Introduction

Energy storage is a key technology for a successful transition to green energy because of the fluctuating and less predictable character of renewable sources (e.g. wind and solar). When thinking about overall energy efficiency, it is important to note that about 40% of the energy is consumed by buildings, which is generally attributed to the space and water heating [1, 2]. Meanwhile, latent heat thermal energy storage (LHTES) technology can play a very important role in the managing of energy consumption [3, 4].

Phase Change Materials (PCMs) are closely associated with TESs. They have been receiving significant attention as potential thermal energy storage mediums, as they have large latent heat of fusion, which causes a high amount of thermal storage, they are capable to absorb and release heat during melting and solidification, respectively [5].

Previous studies on the heat transfer mechanisms in the phase change process within LHTESs show that the convective heat transfer has the main role of heat transfer from heat sources to the phase change front, especially during the melting process [4, 6-8]. So, many attempts undertalen by researchers to improve the melting process by investigating the convective heat transfer.

Seddegh et al. [9] performed a comparative study between cylindrical and conical vertical shell and tube LHTES experimentally and analytically. Since the dominant role of the heat transfer in the upper side of LHTES was the convection, the conical LHTES charged faster than the cylindrical one, but, during the discharching, no significant difference was observed.

A simple method was proposed by Hong et al. [10] to improve the melting phenomenon. The phase change process begins close to the two isothermal heat sources on the vertical wall. In this study, the effect of inverting LHTES in different stages was numerically investigated by employing enthalpy porosity model. The results showed that inverting LHTES in the dimensionless time of 0.4 of complete melting time caused 24.3% increase in the final liquid fraction. This indicated the effect of the convective heat transfer on the melting and presented a technique to control that.

In another study, Hong et al. [11] studied the effect of the angle of an inclined LHTES, the number of discrete heat sources, partial cold wall and aspect ratio on the time of melting. The results showed that the overall time of melting reduces more than 40% for the inclination angle of 0^o, the aspect ratio of 0.05, and 4 discrete heat sources.

Zhao et al. [12] have carried out a numerical as well as an experimental study on the PCM melting phenomenon in a tilted rectangular cavity at deferent angles from zero to 90^o. They employed the

improved Nusselt boundary layer for solving the problem. The liquid fraction, dimensionless height and the final melting time of the PCMs were investigated which were supported by experimental results. The results demonstrated that the shortest final melting time occurred at the tilt angle of 60^{o}.

Dai et al. [13] investigated the melting heat transfer within a cavity heated from its sidewalls. The study was accomplished using the enthalpy based Lattice Boltzmann method (LBM). The results have asserted that the biggest molten fraction was achieved when the melting was being driven from the left and down sides. In addition, they showed if the angle increases, the melting efficiency will be higher.

Kamkari and Amlashi [14] also studied the effect of the angle on the melting behavior of Lauric acid at different Stephan numbers. The results showed that the time of complete melting for 0° and 45° inclined enclosures were respectively about 52% and 37% shorter than that of the vertical enclosure. The authors explained that this phenomenon was attributed to the intensification of the natural convection in the inclined cavity. There have been more studies done on the effect of fins embedded to the LHTES to improve the heat transfer behavior of PCM [9, 15, 16]. a comprehensive literature review regarding enhancement in melting process in LHTES by means of fins can be found in the study by Dhaidan and Khodadadi [17].

Bondareva and Sheremet [18] investigated the heat transfer and the melting-driven flow within a cavity equipped with a local heat-generating source. A finite difference method with the second-order accuracy has been employed to solve governing equations. The effects of the heat generation rate and the buoyancy-driven force have been studied by varying the governing variables such as Rayleigh number, the Stefan number and the Ostrogradsky number. The temperature field and streamlines has been illustrated. The associated results would be applicable in the cooling process of electrical components.

Another study was conducted by Prieto and González [19] on the arrangement (horizontal or vertical) and the thickness of PCM affection on the melting and solidification of a paraffin and fatty acid PCMs in a rectangular panel. Results showed that the vertical arrangement produced slightly higher flow intensity compared to the horizontal arrangement solidfor both during melting and solidification. This was due to the role of the convective heat transfer.

Dadvand et al. [20] investigated the melting of a NePCM close to a heated thin plate in a square cavity. They studied the effect of different positions and nanoparticles concentrations on the

melting performance. The highest melting rate was resulted for the case of the plate at bottom position and the volume fraction of 5%.

Feng et al. [21] carried out a study on the melting in a heated-bottom cavity. In this work, the phenomenon of ice melting heat transfer with copper nanoparticles was numerically modeled using the LBM. Their results were presented in the form of streamlines and isotherms of the various volume fractions of nanoparticles and two different Grashof numbers. The results showed that the enhanced efficiency of the heat transfer attributed significantly to the distribution of nanoparticles in the ice. The results also showed a formation of an asymmetric melting zone for the high concentrated PCMs at the Grashof number of 2.5×10^5.

Arici et al. [22] investigated the phenomenon of the melting of a paraffin wax as a PCM in a square cavity with a mounted fin on the center of the heated wall. The effect of the fin length on the melting rate was examined. In addition, the orientation of the cavity on the melting process was studied. The results shows that as the fin length increases, the melting rate improves impressively at the early time of the melting. In any case, the impact of the fin length on the melting rate reduces after longer heat transfering. It is also inferred that the melting rate can be improved essentially by changing the orientation of the warmed wall in the square cavity.

Bondareva and Sheremet [23] studied numerically the nano-PCM melting in a cavity equipped with copper fins. They were attached to a constant heat-source element. The non-dimensional Navier-Stokes and enthalpy formulation have been employed for the description of the melting front. It was observed that an increase in the nanoparticles fraction causes an improvement in the melting process especially at the initial time of the melting due to an increase in the thermal conductivity.

Ismael [24] studied the role of baffle in a forcrd convection heat transfer process within a channel. The fluid-solid interaction has bee studied for higher and lower Reynolds numbers. The results reveal that the best length of the baffle is 0.2 times the channel height regarding the effective thermal performance.

A cooling system developed for liquefied natural gas in a baffled storage tank is studied by Haddar et al. [25] to demonstrate the the affection of baffles' numbers, position and dimension on the flow charectaristic and thermal behavior of the system. The results show if the baffles locate at the top of the tank, the dimensionless average temperature can be reduced by 36%.

Reviewing literature shows melting in rectangular cavities demonstrates simply close-contact phase change considers a lot of applications in heat storage units such as solar energy systems, nuclear reactors, and geothermal systems [26, 27]. In these configurations, the temperature gradient would cause strong buoyancy-driven flow and a non-uniform melting front. This phenomenon results in unmelted masses of PCM at some parts of the domain. This fact could cause some drawbacks, as we know the amount of stored energy and melted PCM is inextricably bound up. Therefore, the shape and the size of cavities must be investigated precisely, regarding the melting characteristics, ensuring that the optimum heat-storing performance takes place [15].

In the other hand, the preconceived notions that a conductive baffle can improve the performance of a heat storage motivated us to implement this study . So, this numerical study was accomplished to represent how a conductive baffle influences the melting process. To do this, a home-generated FORTRAN cod was developed to model the fluid flow and the heat transfer in a rectangular cavity. Ultimately, the best case including the optimum distance of the baffle from the hot wall and its height will be acknowledged regarding the liquid fraction rate as well as the amount of the heat storage.

2. Methodology

Figure 1 shows the streamlines and liquid-solid front in three different dimensionless times of melting in a rectangular cavity. Since the temperature, set at the left boundary is more than the melting point of gallium; the melting process initiates from the left side and proceeds to the right side of the cavity.

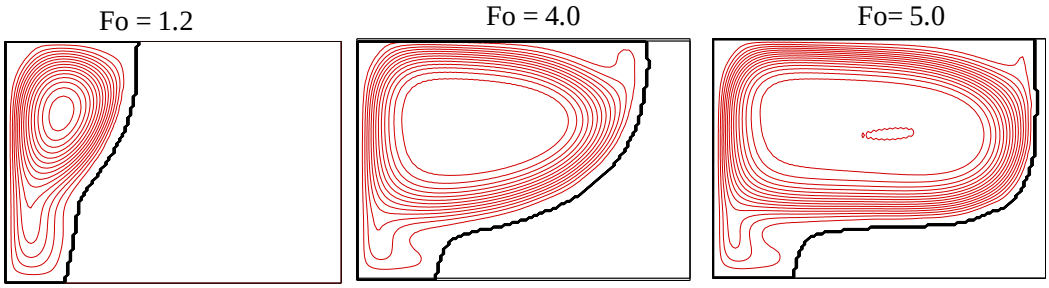

Figure 1: streamlines and liquid-solid front at various dimensionless time of melting in a rectangular cavity.

As it can be seen, the buoyancy-driven convective circuits formed in molten area transfers heat from the left section to the right section of the cavity. They rise up near the left side-wall and then fall down near the liquid-solid front. Therefore, the temperature at the top area is generally higher than the bottom, causes a fast melting rate at the top. This causes a non-uniform melting in the cavity. Therefore, a significant value of PCM remains solidus at the bottom right side of the cavity. This represents an inappropriate melting process and reduces the efficiency of heat-storing system. Hence, the main target of this study is to achieve a uniform liquid-solid front from up to bottom of the cavity in order to improve the melting characteristic and the final liquid fraction. Therefore, a single conductive baffle is embedded on the upper wall of a cavity to control the buoyancy flow and prevent an ununiformed melting front.

Figure 2 shows a sample of symmetric PCM storage used in the domestic building to storage heat from solar water heater (SWH) systems [15, 28]. A supposed section of it consisting of a rectangular cavity with an aspect ratio of *R=0.714*, filled with pure solid gallium. This system is initially at a temperature (T_c) lower than melting point of gallium (T_l). A conductive baffle with a height of LY and the thickness of tx/L=0.01 at a distance of LX from hot wall is embedded on the upper wall. The thermal conductivity of the baffle is the same as the PCM. The left and right vertical sides are held at the constant temperature of T_c and T_h ($T_h > T_l > T_c$). The top and bottom walls of the cavity are supposed to be insulated. The thermal properties of the PCM are listed in Table 1.

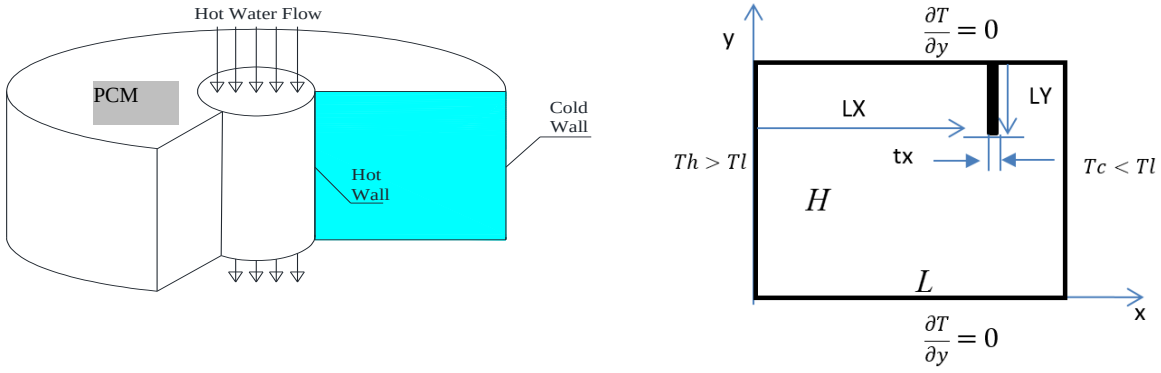

A B

Figure 2: A. Domestic PCM storage [15], B. The physical model of the LHTES cavity with boundary conditions

Table 1: Gallium thermophysical properties

Parameters	Value
Density, ρ	6093 kgm^{-3}
Volumetric thermal expansion coefficient of liquid, β	$1.2\times 10^{-4}{}^{o}C^{-1}$
Thermal conductivity, k	32.0 $Wm^{-1}{}^{o}C^{-1}$
Melting point, T_l	29.78 ^{o}C
Latent heat fusion, h_l	80160 Jkg^{-1}
Thermal diffusivity, α_f	1.38×10^{-5} m^2s^{-1}
Pr	0.0216
c_s/c_f	1.0
k_s/k_f	1.0

The governing equations and the non-dimensional forms are given in equations 1-5. These equations have been translated to the dimensionless form using the variables and dimensionless parameters tabulated in Table 2.

• Continuity:

$$\frac{\partial u}{\partial x}+\frac{\partial v}{\partial y}=0$$

$$\frac{\partial U}{\partial X}+\frac{\partial V}{\partial Y}=0 \qquad (1)$$

• X momentum:

$$\frac{\partial u}{\partial t}+u\frac{\partial u}{\partial x}+v\frac{\partial u}{\partial y}=\frac{1}{\rho_f}\left(-\frac{\partial p}{\partial x}+\mu\nabla^2 u+bu\right)$$

$$\frac{\partial U}{\partial Fo}+U\frac{\partial U}{\partial X}+V\frac{\partial U}{\partial Y}=-\frac{\partial P}{\partial X}+\Pr\nabla^2 U+BU \qquad (2)$$

• Y momentum:

$$\frac{\partial v}{\partial t}+u\frac{\partial v}{\partial x}+v\frac{\partial v}{\partial y}=\frac{1}{\rho_f}\left(-\frac{\partial p}{\partial y}+\mu\nabla^2 v+bv+\rho\beta g(T-T_l)\right)$$

$$\frac{\partial V}{\partial Fo}+U\frac{\partial V}{\partial X}+V\frac{\partial V}{\partial Y}=-\frac{\partial P}{\partial Y}+Pr\nabla^2 V+RaPr\theta+BV \qquad (3)$$

• Energy for PCM:

$$\frac{\partial T}{\partial t}+u\frac{\partial T}{\partial x}+v\frac{\partial T}{\partial y}=\alpha_f\nabla^2 T-\frac{h_l}{c_f}\left(\frac{\partial f}{\partial t}\right)$$

$$\frac{\partial \theta}{\partial Fo}+U\frac{\partial \theta}{\partial X}+V\frac{\partial \theta}{\partial Y}=\nabla^2\theta-\frac{1}{Ste}\left(\frac{\partial f}{\partial Fo}\right) \quad (4)$$

• Energy for conductive baffle:

$$\frac{\partial T}{\partial t}=\alpha_s\nabla^2 T$$

$$\frac{\partial \theta}{\partial Fo}=\frac{\alpha_s}{\alpha_{PCM}}\nabla^2\theta \quad (5)$$

The equations include both fluid dynamics (Navier–Stokes) and energy conservation equations. The Boussinesq approximation for buoyancy is adopted as term of $RaPr\theta$ in the Y-momentum equation as well.

Table 2: The dimensionless parameters using to non-dimensionalize of the equations

Dimensionless parameters	Description
$X = x/H,\ Y = y/H,$	Non-dimensional dimensions
$U = uH/\alpha_f,\ V = vH/\alpha_f,$	Non-dimensional velocities
$\theta = (T - T_l)/(T_h - T_l),$	Non-dimensional temperature
$P = pH^2/\rho\alpha_f^{\ 2},$	Non-dimensional pressure
$Fo = \alpha_f t/H^2$	Fourier number
$B = bH^2/\rho_f\alpha_f$	Dimensionless form of coefficient *b*, Based on the Carman-Kozeny relation [29].
$Ra = g\beta(T_h - T_l)H^3/\nu_f\alpha_f$	Rayleigh number
$Ste = c_f(T_h - T_l)/h_l$	Stefan number
$\mathrm{Pr} = \upsilon_f/\alpha_f$	Prandtl number

The enthalpy-porosity formulation is used to define mathematically the d-liquid phase change process. The dimensionless initial and boundary conditions are expressed in Table 4.

Table 4: The initial and boundary condition

Case	Initial / Boundary condition
Initial time	Fo=0, U=V=0 and θ= -0.18
Left wall	U=V=0 and θ =1
Right wall	U=V=0 and θ = - 0.18
Horizontal walls	U=V=0 and $\frac{\partial \theta}{\partial Y} = 0$
Liquid-solid interface	U=V= θ =0
On the baffle	U=V=0

For control volumes containing a liquid phase of the substance, *f* is set to 1.0, and for control volumes containing solid phase, *f* is set to zero. The control volumes with values of *f* between zero and 1 are assumed to be mushy zone.

The power-law scheme, which is a combination of the central difference and the upwind schemes, is used to discretize the convection terms in the governing equations. The Patankar's SIMPLE algorithm is used to solve the discretized and coupled continuity, momentum and energy equations. A line by line solver based on the tri-diagonal matrix algorithm is used to solve iteratively the algebraic discretized equations [30]. The enthalpy porosity method proposed by Voller et al. [31] was employed to model the liquid-solid interface.

3. Grid and Time Step Study

In order to determine the proper grid size and time step, a grid independency study is performed for various grid sizes with time step size in the range of 0.01 to 1.0. The liquid fraction is elected as the monitoring variable. The liquid fraction is the volume of molten substance to the volume of the cavity. Finally, the grid size of 110×125 grids with a time step of 0.1 supported a sufficient accuracy, see the Figure 3. The convergence criteria was set on the maximum residual equal to 10^{-6} for the continuity equation.

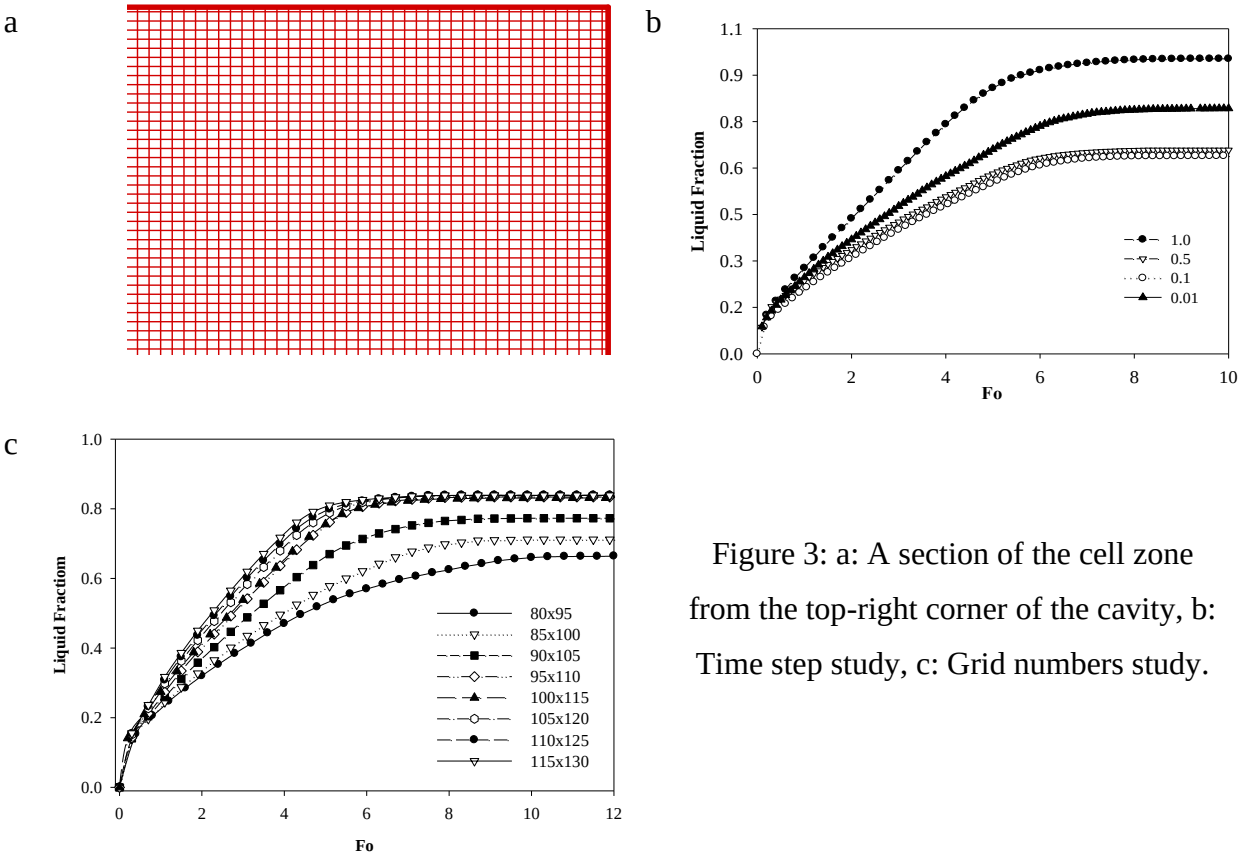

Figure 3: a: A section of the cell zone from the top-right corner of the cavity, b: Time step study, c: Grid numbers study.

The validation test was done in comparison with previous literature, the numerical study by Brent *et al*. [32] and the experiment of Gau and Viskanta [26] on similar LHTES for the boundary conditions of $T_h=38^0C, Tc=28.3^0C$, the initial temperature of 28.3^0C, and the domain size of 63.6×88.9 mm^2 ($R=0.714$). Figure 4 shows the simulation of melting front at different times inside the cavity against the results of the mentioned papers. The maximum deviation was shown on the figure. It can be observed that the agreement is reached with the maximum deviation of 5%.

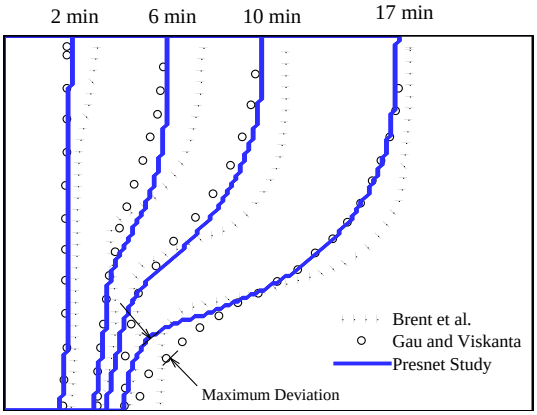

Figure 4: Numerical code validation of the present study with the numerical results of Brent et al. [32] and the experimental study of Gau and Viskanta [26].

4. Results and Discussion

The numerical results with the configuration shown in Figure 1 are presented in two parts; first, the effect of the conductive baffle's location on the heat transfer rate, the flow, and the phase change phenomena is studied. The computations are performed for eight-different dimensionless distance of baffle from the hot wall, namely LX/L=0.2, 0.3, 0.4, 0.5, 0.6, 0.7, and 0.8. Regarding the higher melting rate and the amount of heat energy storage, the most proper location of the conductive baffle will be reported. Second, the effect of the dimensionless height of the baffle, including LY/L=0.2, 0.3, 0.4, and 0.5, will be studied on the melting process. In both cases, the streamlines and isotherms in the melted region, the liquid fraction in the cavity, and the average Nusselt number on the hot wall are demonstrated as a function of the dimensionless time. Throughout the study, the Rayleigh number is considered to be constant and equal to 10^6.

Figures 5-8 show the streamlines and liquid-solid front during the melting process for different baffle locations. At the early time of melting, a vorticity nucleus triggered near the left sidewall of the cavity. In this time, there is not any remarkable difference among the cases, see figure 5. However, as time elapses, some cases represent a more fast proceeding of the liquid-solid front, see figure 6. For example, for the cases of LX/L= 0.5 to 0.8, since the baffle is located at a far position from the hot sidewall, the buoyancy-driven vorticity has a sufficient area to operate. Therefore, the ever-strengthening circulating flow absorbs the heat efficiently from the hot wall and releases it near the liquid-solid front. The point is that for the cases LX/L= 0.2 and 0.3 since the vorticity encounters the baffle at the top, it has to proceed through the down part of the cavity. Therefore, the liquid-solid front took a more uniform form from the top to the bottom of the cavity in comparison to the other cases.

In other words, by embedding a conductive baffle on the upper wall of the cavity, new boundary conditions are imposed on the domain. Because of the no-slip condition on the solid baffle, the molten flow has to be smoothly adapted with the new conditions. Subsequently, different styles of melting take place depending on the gap between the hot wall and the baffle. Actually, the baffle lets heat pass through it via conduction but obstructs the convective heat transfer.

Figure 7 shows that in some cases the baffle even dampens the melting process. For LX/L= 0.2 and 0.3, the lowest amount of molten represents at the time Fo=5.0. It seems that the baffle splits the firstly big strong vorticity into the secondly small ones. For LX/L= 0.6 to 0.9, a strong vorticity covers an extensive area of the cavity, reaching the maximum stream function value, $|\psi|=1.33$.

Figure 8 represents the streamlines and liquid-solid front when the melting process ends in a steady-state condition. Without a baffle, large vorticity formed between the left and the right side of the cavity. Due to the buoyancy affections, the fluid flow rises up near the left hot wall and falls down near the melting front. Therefore, a clockwise circulation driven by the convective heat transfer forms. This flow plays the main role of heat transfer through the PCM. However, because of a cold temperature lower than the melting point on the right wall, the flow cools down along the liquid-solid front. As a result, its temperature drops and is not high enough to melt the PCM at the right bottom of the cavity. Therefore, the flow completely reverses its direction into the hot wall before it reaches the bottom of the cavity. The result is a remained solidus PCM in this region. With the baffle though new boundary conditions imposed on the domain. Tha baffle now forces the circulating buoyancy-driven flow to pass through the gap that is between the baffle and the bottom of the cavity. This event is exactly the thing that is wanted to happen.

In the cases of LX/L=0.2 to 0.4, the baffle causes to form two small vorticities one at the baffle left side near the bottom of the cavity and another at the baffle right side near the top wall. The left one transfers heat from the hot wall to the baffle and the PCM, and the right one transfers heat from the baffle to the liquid-solid front. This vorticity is not strong enough to penetrate more into the solid PCM at the right section of the cavity and the melting process stops unexpectedly, while a significant amount of PCM remained solidus in the right section.

For the case of LX/L=0.4, since the more amount of PCM gets engaged in the melting process at the left section, the higher temperature gradient brings about and a stronge vorticity forms between the hot wall and the baffle. On the contrary, the right one is not as strong as the left one. Accordingly, a larger mass of PCM remains solidus. (see the solid color at the right region, figure 8). Due to this, the unmelted PCM is even more than what is for the case without baffle.

For LX/L=0.5, the baffle is certainly located at the centerline of the cavity, there are equal spaces on the sides of the baffle for forming the circulating flows. This is the only case in which a strong circulating flow remains at the right side of the baffle. The reason may rely on that in the first half

time of melting, due to a sufficient area between the hot wall and the baffle, an effective buoyancy-driven flow and heat transfer happens at the left section (see figure 7), which results in a significant temperature rise of the baffle. As a result, a significant temperature gradient occurs between the baffle and the right wall, which makes a remarkable melting proceeding at the right part.

For LX/L=0.6, 0.7, and 0.8, more solid PCM is involved in the buoyancy-driven flow at the left side of the baffle. As a result, the temperature of the baffle is lower than that in the case of LX/L=0.5. Therefore, the less and less temperature gradient takes place between the baffle and the cold wall.

For the case of LX/L=0.9, since there is a large amount of solid PCM between the hot wall and the baffle, the downwelling flow along with the baffle, resembling the case of the cavity without baffle, is not hot enough to melt the PCM at the bottom right corner of the cavity. Therefore, a mass of PCM remains solid at the right-bottom of the cavity.

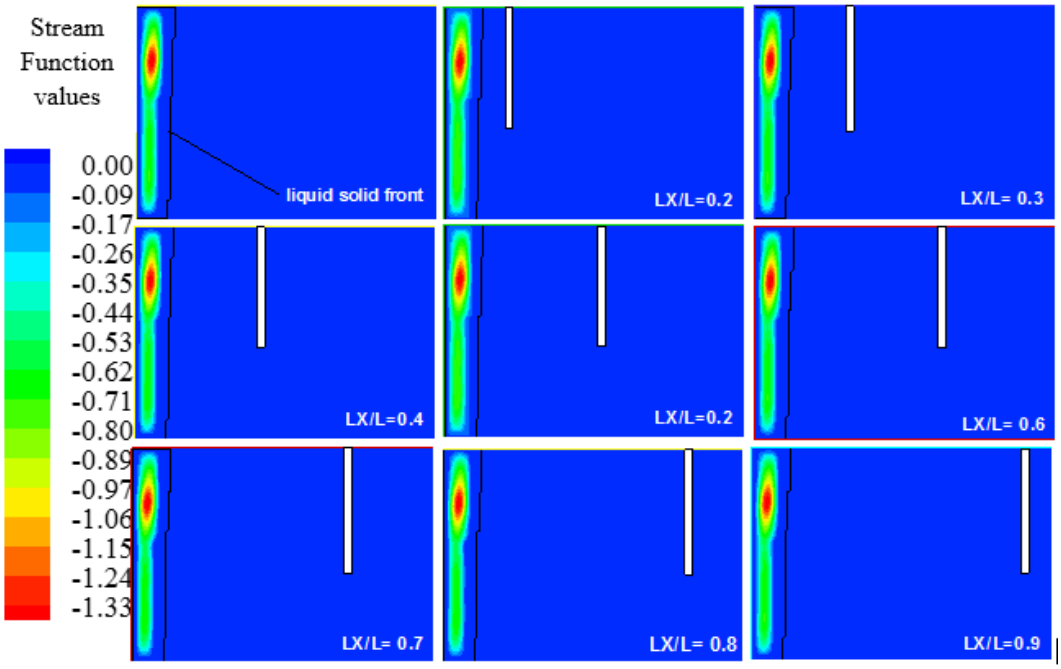

Figure 5: streamlines and liquid-solid front in the early time of melting for various baffle locations

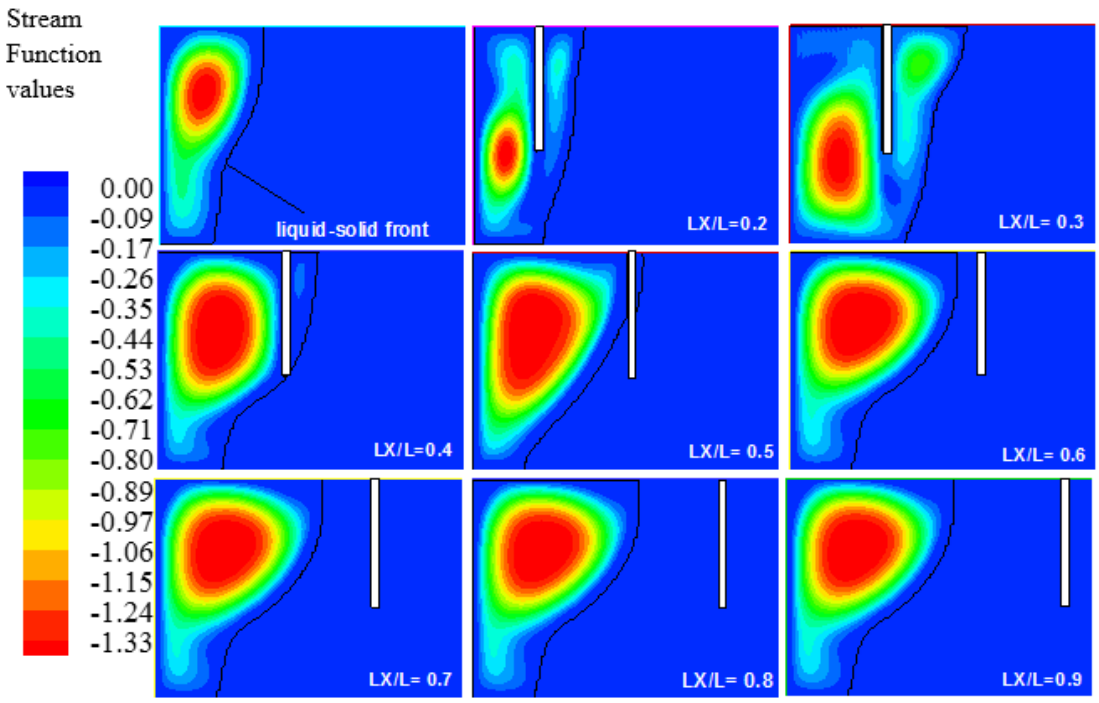

Figure 6: Streamlines and liquid-solid front in the time of Fo=2.5 for various baffle locations

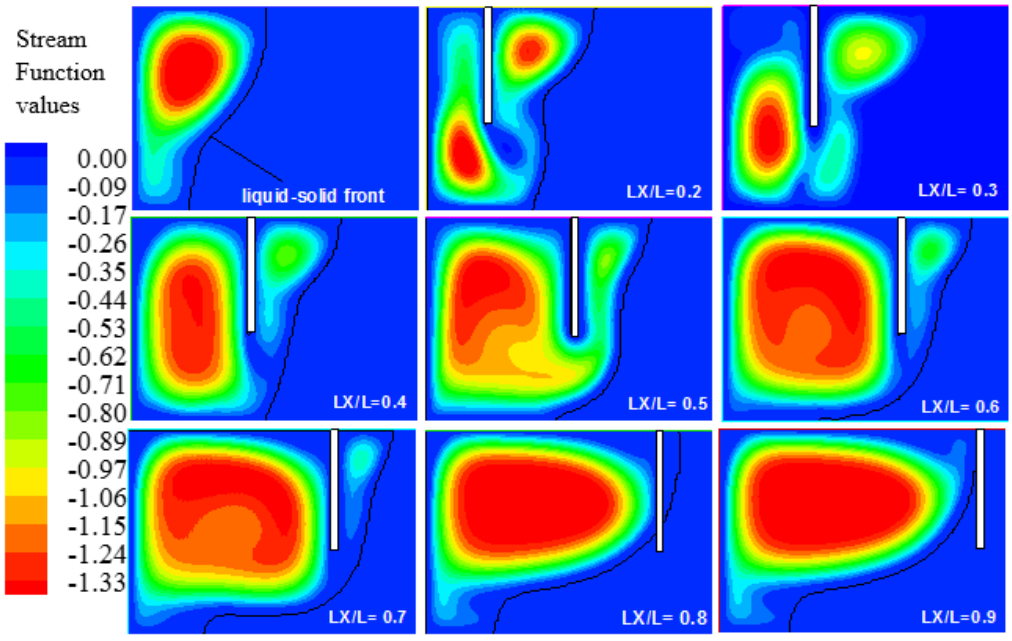

Figure 7: Streamlines and liquid-solid front in the time of Fo=5 for various baffle locations

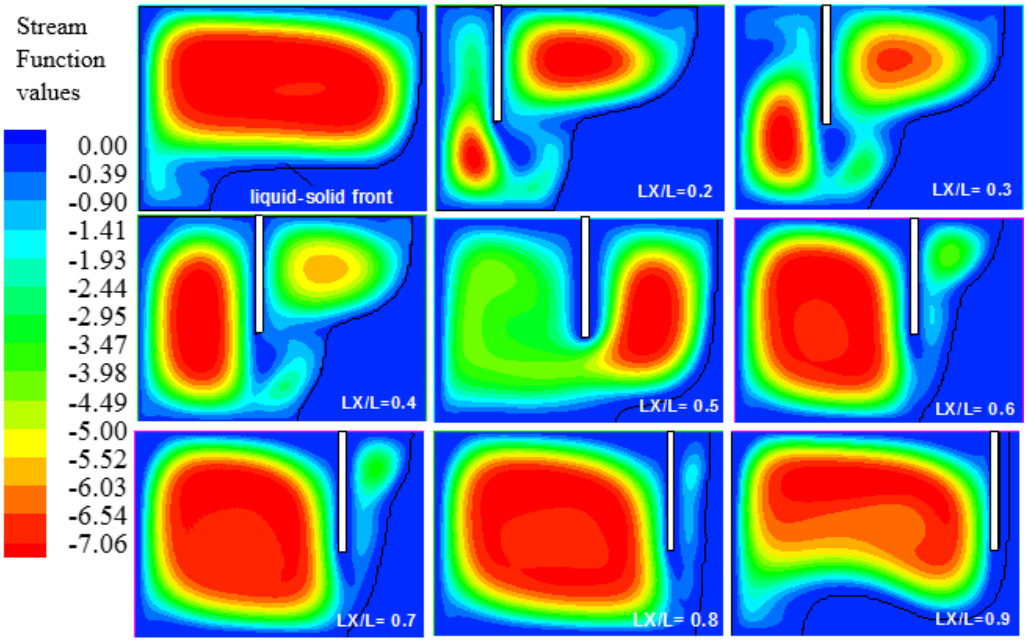

Figure 8: streamlines and liquid-solid front in the end time of melting for various baffle locations

Figures 9-12 show the isotherms and liquid-solid front during the melting process for different baffle locations. At the early time of melting, the isotherms and the liquid-solid front represents a straight pattern formed parallel to the hot wall, see figure 9. However, as time elapses since the convective mechanism plays the main role of heat transfer, the shape of isotherms and the liquid-solid front changes to the curve style. By looking at the isotherms graph the polynomial cubic function crosses the mind ($y=ax^3+bx^2+cx+d$).

As an inevitable certain result, a non-uniform melting proceed at the top compare to the bottom section of the cavity, see figure 10. In this state, the affection of conductive baffle is significant. For cases in which, the front has reached the baffle, the isotherms take parallel form along with the baffle. An straight and parallel shapes reveal the role of conductive heat transfer in this area.
The results show that generally the baffle causes not only the isotherms' pattern to change, but also the shape of isotherms at the leftside being completely different from them at the right side, it can be inferred from figure 11 evidently. In other words, the baffle shifts the cubical parabola down to the bottom of the cavity. The corresponding affection of the baffle on the liquid-solid front discussed in the previous section.
Figure 12 represents the isotherms and the liquid-solid front when the melting ends in the steady-state condition. Without the Baffle, a non-uniform liquid-solid front is observed at the end. This

condition results in a mass of non-melted PCM at the right-bottom corner of the cavity. In the case of LX/L=0.2 and 0.3, the straight and parallel lines of isotherms are formed along with the baffle at the left side of the baffle, confirming the dominant conduction mode of the heat transfer at this section. But, at the lower region in which convection heat transfer is the dominant mode, the isotherms take curved forms.

In the case of LX/L=0.5, the isotherms represent more and more curved forms at the left side, since the convection heat transfer becomes stronger. At this time, the temperature gradient between the baffle and the cold wall causes a circulating flow derived by convection which brings about a non-uniform liquid-solid front at the right side of the cavity. However, it is observed that more PCM melts in comparison to the case without baffle.

For LX/L=0.6, 0.7, and 0.8 a strong heat transfer convection occurs at the region between the baffle and the hot wall. But, at the right side of the baffle, a weak temperature gradient generates a poor convective heat transfer which is not strong enough to melt the entire solid PCM in this region.

The baffle generally obstructs the convection flow at the top of the cavity and pushes it down. Subsequently, the flow has to pass through the limited space between the baffle and the bottom wall of the cavity and melts various amounts of PCM, depends on the baffle's location.

In the case of LX/L=0.9, more PCM gets involved in the circulating flow at the left side of the cavity. Therefore, a non-uniform melting occurs within the cavity.

The morphology of the melting front reveals that the most uniform melting process belongs to the LX/L=0.8. Therefore, the most final liquid fraction also associates to this case.

The final liquid fraction, the final dimensionless time of melting, and the maximum stream function of the flow in the molten PCM for various baffle locations are tabulated in table 4. These data show that the case of the cavity without baffle represents the shortest time with a liquid fraction of 0.788, which is not the the efficient case. The most liquid fraction, the most stored energy obtains. Regarding this, the case of LX/L=0.8, with the liquid fraction of 0.95, results in the best melting characteristic and hence the highest amount of the stored heat.

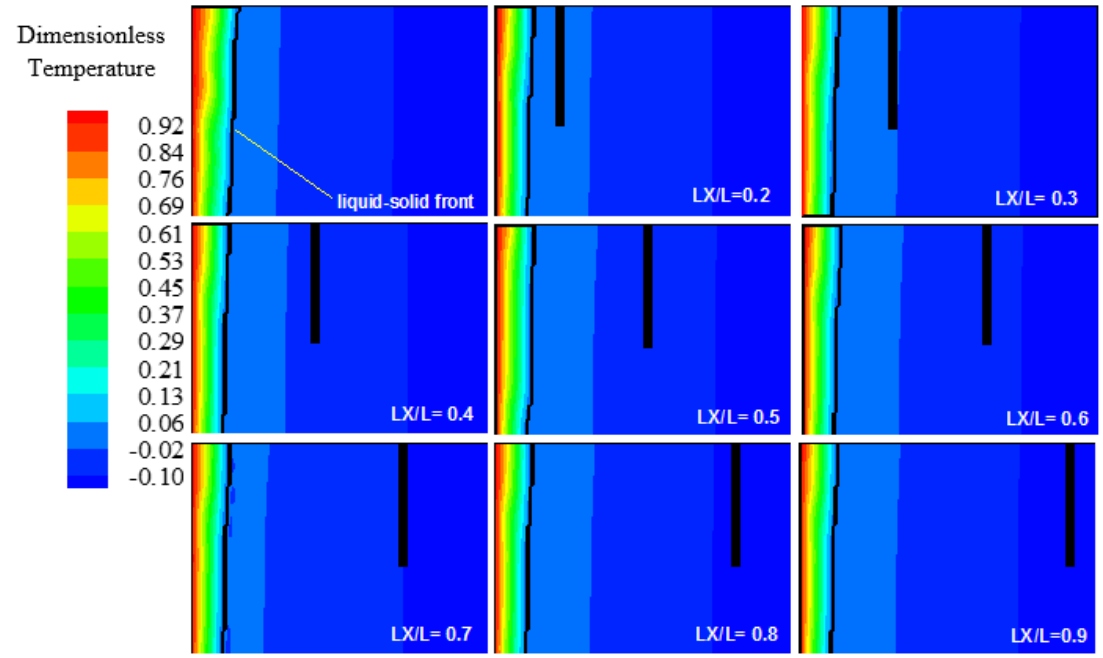

Figure 9: Isotherms and liquid-solid front in the early time of melting for various baffle location

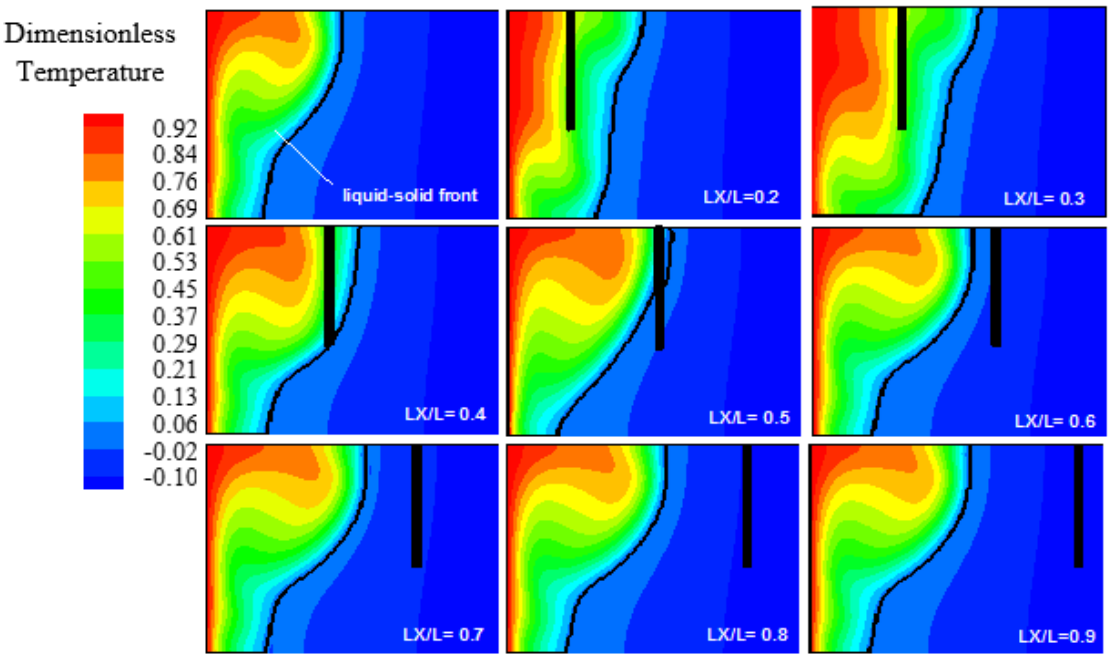

Figure 10: Isotherms and liquid-solid front in the time of Fo=2.5, for various baffle locations

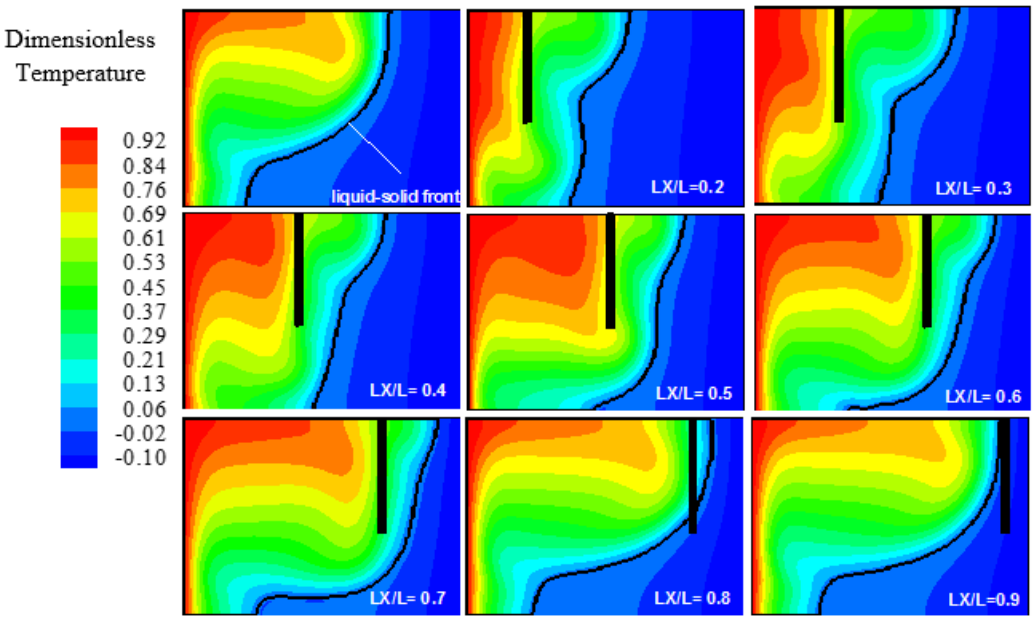

Figure 11: Isotherms and liquid-solid front in the time of Fo=5 for various distances from hot wall (LY/L=0.4)

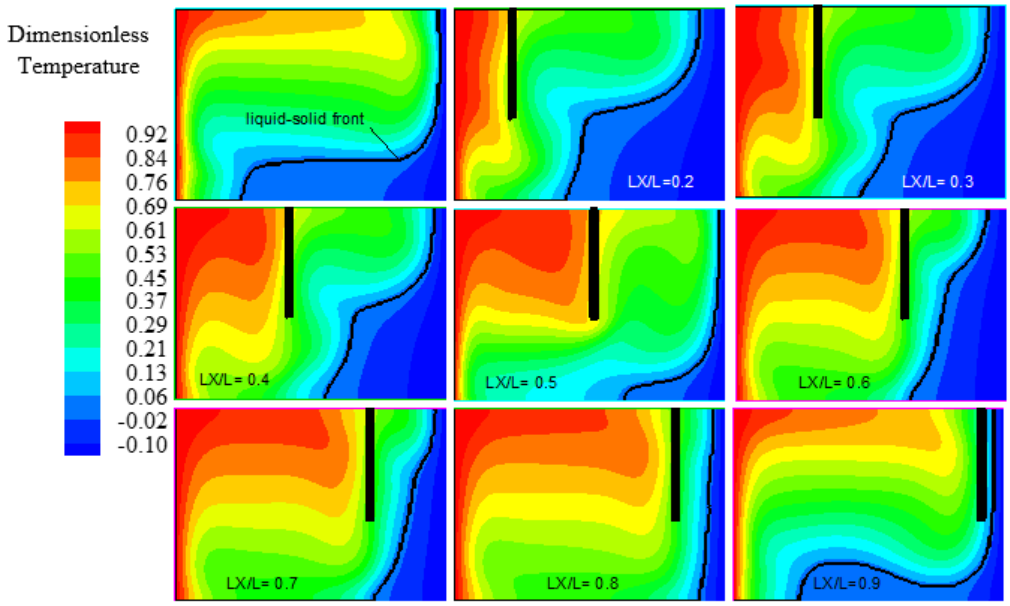

Figure 12: Isotherms and liquid-solid front in end time of melting for various distances from hot wall (LY/L=0.4)

Table 4: Final liquid fraction and dimensionless time of melting (LY/L=0.4)

Baffle location (LX/L)	Final liquid fraction	Final dimensionless time	Ψ_{max}
0.2	0.672	16.0	-5.41

0.3	0.728	17.9	-6.76
0.4	0.780	10.4	-7.15
0.5	0.882	9.0	-12.6
0.6	0.886	8.4	-6.52
0.7	0.891	8.1	-6.63
0.8	0.950	9.5	-7.10
0.9	0.860	9.5	-7.13
Without baffle	0.788	7.6	-7.56

Figure 13 represents the variation of liquid fraction during the dimensionless time of the melting. Steady trend can be observed for the cases of LX/L=0.2 to 0.4. However, a dramatic rise of liquid fraction is integrated with the cases of 0.5 to 0.9 at the time Fo=5.0. Moreover, The high rate of melting can be found in the cases of 0.5 to 0.9 in comparison with the others.

To conclude, the maximum amount of liquid fraction can be observed for LX/L=0.8. This case brings about the 20% improving in liquid fraction compare to the case of without baffle.

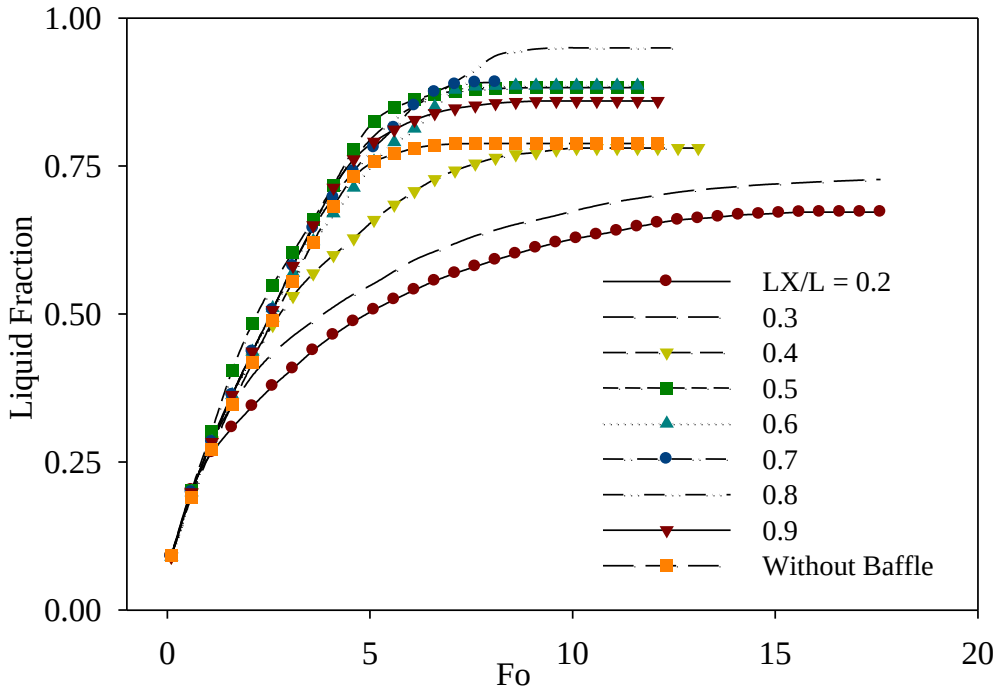

Figure 13: Liquid Fraction versus dimensionless time for various baffle locations (LY/L=0.4)

The average Nusselt number on the hot wall indicating the heat transfer rate is reported to demonstrate the amount of the heat transfers through the cavity. It is calculated by equation 6.

$$\overline{Nu} = -\frac{\int \frac{\partial \theta}{\partial X} dY}{Y} \tag{6}$$

The variation of the average Nusselt number versus the dimensionless time is depicted in Figure 8. A large value of Nusselt number can be observed at the initial time of the melting when the conduction heat transfer is dominant and the high-temperature gradient exists between the hot wall and the adjacent PCM. As time elapses, the average Nusselt number decreases dramatically as the convection heat transfer becomes dominant and makes a decline in the temperature gradient. A considerable fluctuation can be observed for LX/L=0.5 at Fo=4.8 when the liquid-solid front shifts from the left to the right side of the baffle. Generally, downward trends can be seen for all the average Nusselt numbers. However, for the cases of 0.6 to 0.8, the falling takes place at a greater time. For example for the case of LX/L=0.8, the sharp falling happens at the dimensionless time of 0.7. The results show, constant values of the average Nusselt number take place at the steady state condition when the melting process ends. Moreover, the low values of the average Nusselt numbers at the end of the melting represents the poor heat transfer on the hot wall. This event, actually, might be associated with the lowest values of the stream functions in Table 2. Surprisingly, if a cooling process on the hot wall is intended, the case without baffle demonstrates a good heat transfer rate as it represents the highest value of Nusselt numbers in the steady-state condition. To conclude, taking into account both the amount of the energy storage and the heat transfer rate, the case of LX/L=0.5 represents the best characteristic of melting process.

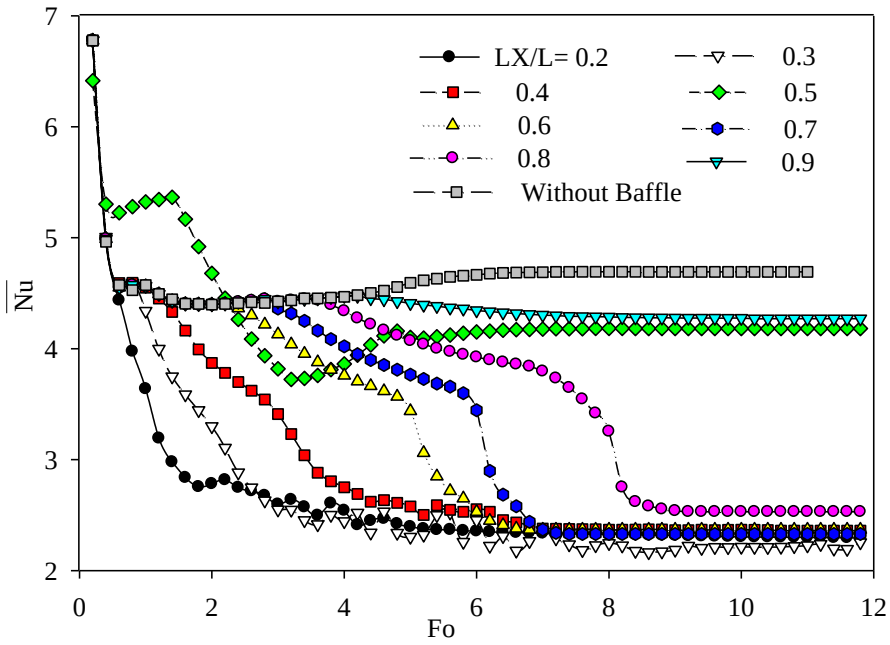

Figure 8: Average Nusselt number versus dimensionless time for various baffle distances from hot wall (LY/L=0.4)

In this section, for a constant dimensionless distance of the baffle from the hot wall, namely LX/L=0.8, the effect of the baffle height on the melting process is investigated. Figure 9 represents the streamlines as well as isotherm lines at the end of the melting time for the various dimensionless height of the baffle. It also shows the liquid-solid front remarked by a thick line on the isotherms lines.

As it can be seen, for the case of LY/L=0.2, asymmetric vortices develop through the cavity, causing a non-uniform liquid-melting front at the end of the melting. The point is that in this case, like the case without baffle, the downwelling cold flow adjacent to the liquid-solid front would not be hot enough to melt the solid PCM at the bottom-right corner of the cavity. For the height of LY/L=0.3, the baffle pushes the top convective flow down which causes hot flows penetrate more deeply to the solid PCM at the bottom of the cavity. For the height of LY/L=0.4, the baffle brings about a symmetric large vorticity at the left side region of the baffle. Accordingly, a uniform liquid-solid front is generated parallel to the cold wall. The same condition can be observed in the case of LY/L=0.5. Apart from the case of LY/L=0.2, the results show that the changing height of the baffle from 0.3 to 0.5 generate a uniform melting front. Figure 10 confirms this idea, as it can be seen in the cases of LY/L=0.3 to 0.5, the liquid fraction can be improved by approximately 18%, compared to the case without baffle.

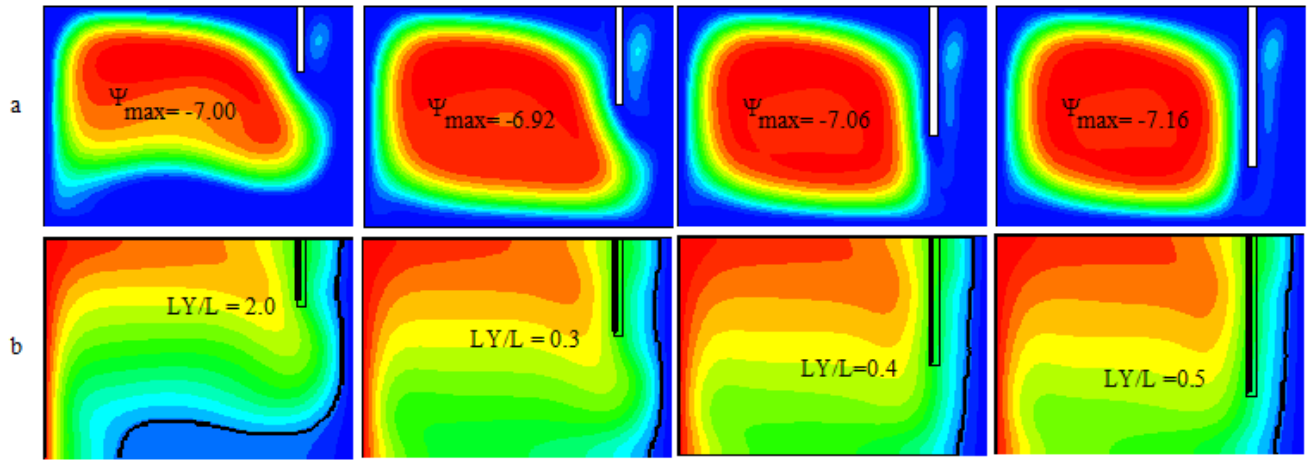

Figure 9: a-Streamlines, b- Isotherms and solid-liquid front at the end of melting for various baffle's heights (LX/L=0.8)

The variation of the average Nusselt number versus the dimensionless time for various heights of the baffle is depicted in Figure 11. Generally, same falling trends can be observed for all the various heights of the baffle up to Fo=4.0. A considerable falling can be observed for LY/L=0.4 and 0.5 near the end of the melting. These fallings might be associated with the fact that the vorticity which covers the whole cavity, see Figure 9, causes a good heat transfer rate from the hot wall to the solid PCM. As a result, at the steady state condition, more amount of PCM melts and makes a reduction in the temperature gradient as well as the average Nusselt number.

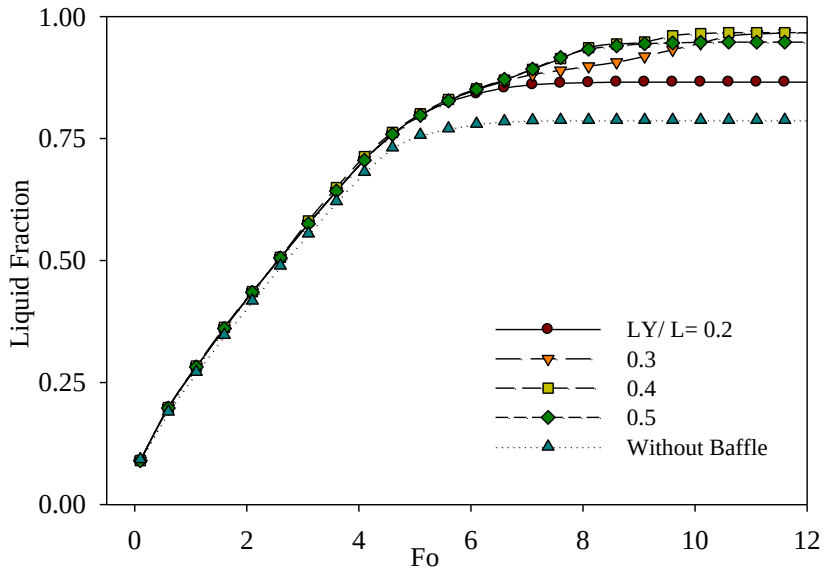

Figure 10: Liquid Fraction versus dimensionless time for various baffle height at Ra=10^6

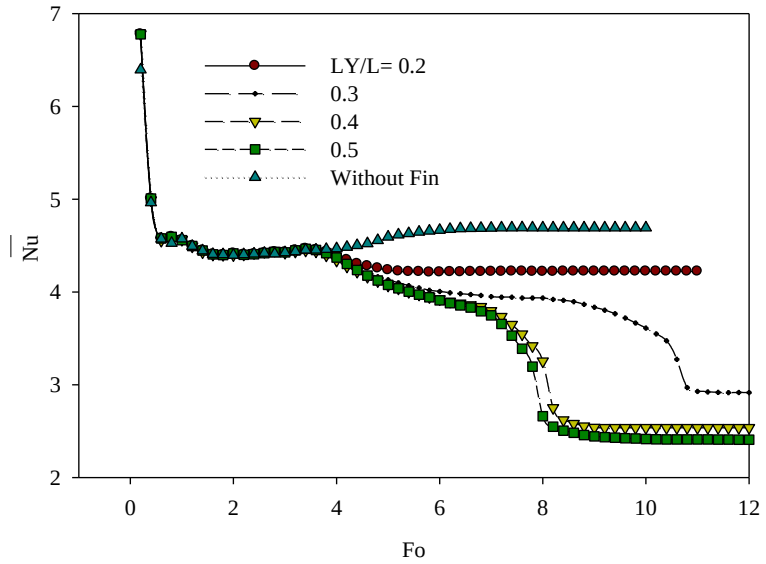

Figure 11: Average Nusselt number versus dimensionless time for various baffle height (LX/L=0.8)

5. Conclusion

In this study, the effect of a single conductive baffle's location and height attached to the upper wall of a rectangular cavity on the melting process of gallium was investigated numerically. The numerical computations were performed for different dimensionless baffle's locations (LX/L=0.2 to 0.8) and heights (LX/L=0.2 to 0.4). All cases were compared with the cavity without baffle as a reference case. The numerical results demonstrated the isotherm lines including melting front,

streamlines, liquid fraction, and average Nusselt number on the hot wall. Significant influences on the related variables were observed by changing the baffle's location and the height. To conclude, the final liquid fraction for the case of LX/L=0.8 reveals the highest rate of the melting compared to the other cases. Meanwhile, the final liquid fraction significantly decreased for LX/L=0.2 to 0.4 but increased for LX/L=0.5 to 0.9 compared to the case of the cavity without baffle. It was shown that the most heat transfer rate on the hot wall was observed in the case of the cavity without baffle. However, taking into account both the amount of the energy storage and the heat transfer rate, the case of LX/L=0.5 represented the best characteristic. Overall, this study remarks a low-cost, high effective and practical methodology to improve the melting behavior of PCM in rectangular cavities.

References

[1] K. Amasyali, N.M. El-Gohary, A review of data-driven building energy consumption prediction studies, Renewable and Sustainable Energy Reviews, 81, 1192-1205,(2018).
[2] A. Andreozzi, B. Buonomo, D. Ercole, O. Manca, Solar energy latent thermal storage by phase change materials (PCMs) in a honeycomb system, Thermal Science and Engineering Progress, 6, 410-420,(2018).
[3] Y. Lin, Y. Jia, G. Alva, G. Fang, Review on thermal conductivity enhancement, thermal properties and applications of phase change materials in thermal energy storage, Renewable and sustainable energy reviews,(2017).
[4] M.S. Mahdi, H.B. Mahood, A.A. Khadom, A.N. Campbell, M. Hasan, A.O. Sharif, Experimental investigation of the thermal performance of a helical coil latent heat thermal energy storage for solar energy applications, Thermal Science and Engineering Progress, 10, 287-298,(2019).
[5] L. Zhang, J. Dong, Experimental study on the thermal stability of a paraffin mixture with up to 10,000 thermal cycles, Thermal Science and Engineering Progress, 1, 78-87,(2017).
[6] M. Arıcı, E. Tütüncü, M. Kan, H. Karabay, Melting of nanoparticle-enhanced paraffin wax in a rectangular enclosure with partially active walls, International Journal of Heat and Mass Transfer, 104, 7-17,(2017).
[7] R.Y. Farsani, A. Raisi, A.A. Nadooshan, S. Vanapalli, Does nanoparticles dispersed in a phase change material improve melting characteristics?, International Communications in Heat and Mass Transfer, 89, 219-229,(2017).
[8] Ł. Wardziak, M. Jaworski, Computer simulations of heat transfer in a building integrated heat storage unit made of PCM composite, Thermal Science and Engineering Progress, 2, 109-118,(2017).
[9] S. Seddegh, S.S.M. Tehrani, X. Wang, F. Cao, R.A. Taylor, Comparison of heat transfer between cylindrical and conical vertical shell-and-tube latent heat thermal energy storage systems, Applied Thermal Engineering, 130, 1349-1362,(2018).
[10] Y. Hong, W.-B. Ye, S.-M. Huang, M. Yang, J. Du, Thermal storage characteristics for rectangular cavity with partially active walls, International Journal of Heat and Mass Transfer, 126, 683-702,(2018).
[11] Y. Hong, W.-B. Ye, S.-M. Huang, J. Du, Can the melting behaviors of solid-liquid phase change be improved by inverting the partially thermal-active rectangular cavity?, International Journal of Heat and Mass Transfer, 126, 571-578,(2018).

[12] J. Zhao, J. Zhai, Y. Lu, N. Liu, Theory and experiment of contact melting of phase change materials in a rectangular cavity at different tilt angles, International Journal of Heat and Mass Transfer, 120, 241-249,(2018).
[13] R. Dai, Q. Bian, Q. Wang, M. Zeng, Evolution of natural convection melting inside cavity heated from different sides using enthalpy based lattice Boltzmann method, International Journal of Heat and Mass Transfer, 121, 715-725,(2018).
[14] B. Kamkari, H.J. Amlashi, Numerical simulation and experimental verification of constrained melting of phase change material in inclined rectangular enclosures, International Communications in Heat and Mass Transfer, 88, 211-219,(2017).
[15] A.M. Abdulateef, S. Mat, J. Abdulateef, K. Sopian, A.A. Al-Abidi, Geometric and design parameters of fins employed for enhancing thermal energy storage systems: a review, Renewable and Sustainable Energy Reviews,(2017).
[16] A.H. Al-Waeli, H.A. Kazem, M.T. Chaichan, K. Sopian, Experimental investigation of using nano-PCM/nanofluid on a photovoltaic thermal system (PVT): Technical and economic study, Thermal Science and Engineering Progress, 11, 213-230,(2019).
[17] N.S. Dhaidan, J. Khodadadi, Improved performance of latent heat energy storage systems utilizing high thermal conductivity fins: A review, Journal of Renewable and Sustainable Energy, 9, 034103,(2017).
[18] N.S. Bondareva, M.A. Sheremet, Flow and heat transfer evolution of PCM due to natural convection melting in a square cavity with a local heater, International Journal of Mechanical Sciences, 134, 610-619,(2017).
[19] M. Prieto, B. González, Fluid flow and heat transfer in PCM panels arranged vertically and horizontally for application in heating systems, Renewable Energy, 97, 331-343,(2016).
[20] A. Dadvand, N.H. Boukani, M. Dawoodian, Numerical simulation of the melting of a NePCM due to a heated thin plate with different positions in a square enclosure, Thermal Science and Engineering Progress, 7, 248-266,(2018).
[21] Y. Feng, H. Li, L. Li, L. Bu, T. Wang, Numerical investigation on the melting of nanoparticle-enhanced phase change materials (NEPCM) in a bottom-heated rectangular cavity using lattice Boltzmann method, International Journal of Heat and Mass Transfer, 81, 415-425,(2015).
[22] M. Arıcı, E. Tütüncü, H. Karabay, A. Campo, Investigation on the melting process of phase change material in a square cavity with a single fin attached at the center of the heated wall, The European Physical Journal Applied Physics, 83, 10902,(2018).
[23] N. Bondareva, M. Sheremet, Natural convection melting of nano-enhanced phase change material in a cavity with finned copper profile, in: MATEC Web of Conferences, EDP Sciences, 2018.
[24] M.A. Ismael, Forced convection in partially compliant channel with two alternated baffles, International Journal of Heat and Mass Transfer, 142, 118455,(2019).
[25] M. Haddar, M. Hammami, M. Baccar, Numerical study of steady natural convection in a liquefied natural gas cylindrical storage tank equipped with baffles, Proceedings of the Institution of Mechanical Engineers, Part A: Journal of Power and Energy, 0957650919870927,(2019).
[26] C. Gau, R. Viskanta, Melting and solidification of a pure metal on a vertical wall, Journal of Heat Transfer, 108, 174-181,(1986).
[27] R.Y. Farsani, A. Raisi, A.A. Nadooshan, S. Vanapalli, The effect of a magnetic field on the melting of gallium in a rectangular cavity, Heat transfer engineering, 1-13,(2017).
[28] J.H. Nicodemus, J.H. Smith, H. Goldstein, Numerical simulations of storage-side natural convection to an immersed coiled heat exchanger with baffle-shrouds, Solar Energy, 182, 304-315,(2019).
[29] J. Garandet, T. Alboussiere, R. Moreau, Buoyancy driven convection in a rectangular enclosure with a transverse magnetic field, International Journal of Heat and Mass Transfer, 35, 741-748,(1992).
[30] S. Patankar, Numerical heat transfer and fluid flow, CRC press, (1980).

[31] V. Voller, Fast implicit finite-difference method for the analysis of phase change problems, Numerical Heat Transfer, 17, 155-169,(1990).
[32] A. Brent, V. Voller, K. Reid, Enthalpy-porosity technique for modeling convection-diffusion phase change: application to the melting of a pure metal, Numerical Heat Transfer, Part A Applications, 13, 297-318,(1988).